International Journal of Advanced Research in Engineering Technology & Science

ISSN: 2349-2819

Email: editor@ijarets.org Volume-9, Issue-2 February – 2022 www.ijarets.org

SYNTHESIS OF NANO FERRITES WITH THE HELP OF WET CHEMICAL METHOD

Shiksha Hooda

Research Scholar in Kalinga University

Abstract:

The synthesis of Mn Zn ferrite nanoparticles was accomplished by beginning with two distinct chemical compounds: oxides as the solid material and metal salts in solution. This was accomplished through the precursor method with hydrazine oxalate ligand and the auto combustion self-decomposition technique. The methods of X-ray diffraction (XRD), scanning electron microscopy (SEM), and pulse field magnetic hysteresis loop tracing were utilised in order to investigate the crystallite size, microstructure, and magnetic properties of the ferrites that were obtained from oxides and metal salts, respectively. The investigation's findings demonstrated that a single phase ferrite may be produced without the need for any post-calcinations. On the other hand, the crystallite size of the oxide sample that was auto-combusted was 24 nm, which was finer than the crystallite size found using the wet chemical approach (43nm). The magnetization of the wet chemically produced Mn Zn ferrite, which had a bigger crystallite size, was 53.4 emu/g, which was much higher than the magnetization of the oxide nanoparticles, which was 39.6 emu/g.

keywords: *nanoparticles, wet chemical, method*

INTRODUCTION

The most common use is for magnetic nanoparticles composed of spinel ferrites. These multipurpose ceramic compounds may be used for a wide variety of applications, including magnetic recording, transformers, transmission devices, and even uses in the medical field. One of the most significant subcategories of soft magnetic ferrite is composed of Mn–Zn ferrites that have a spinel structure. The quantity and distribution of magnetic (Mn2+, Fe2+, and Fe3+) and nonmagnetic (Zn2+) ions in the octahedral and tetrahedral sites in the crystal lattice, which, in turn, rely on the technique of synthesis and other factors, are connected with the behaviour of ferrites in a magnetic field. High saturation magnetization, high magnetic permeability, high electrical resistance, and biocompatibility are some of the characteristics that may be found in Mn Zn ferrite. When it comes to the production of high-quality Mn–Zn ferrite materials, having perfect control over the chemical composition as well as the distribution of particle size is essential. In the past, large-scale commercial production of Mn–Zn ferrite powders were traditionally made by the use of a ceramic process that involved solid phase reactions at elevated temperatures. The process has a number of drawbacks, the most significant of which are inhomogeneities non chemistry and phase composition, in addition to vast particle size dispersion. In recent years, several unique wet-chemical processes have been created. Some examples of these technologies are co precipitation, precursor, hydrothermal, and sol–gel. The limitations of the ceramic approach are investigated and attempted to be circumvented through the use of two alternative beginning procedures in the present work. The first technique involves using a ball mill to grind up the solid oxides, followed by treating them with a ligand in order to produce a precursor. This precursor is then auto-combusted in order to generate the ferrite materials. In the second approach, a solution of metal salts is first prepared, then

treated with the same ligand, and then auto-combusted to produce ferrites. We examined and analysed the microstructure as well as the magnetic characteristics of the Mn Zn ferrite that was synthesised by these two approaches, which are comparable with regard to the occurrence of a self-propagating reaction upon ignition.

EXPERIMENTAL SECTION

Nanoparticles of Mg-Zn ferrite (MgxZn1-x Fe2O4, with values of x equal to 0.2, 0.4, 0.6, and 0.8) were produced by the use of a precursor technique. In this particular synthesis, the chemicals magnesium nitrate Mg(NO3)2 6H2O, zinc nitrate Zn(NO3)2 6H2O, and ferric nitrate Fe(NO3)3 9H2O were utilised as starting materials. All of the compounds were of a quality suitable for analytical use. In order to achieve a solution that is transparent, a stoichiometric amount of Mg(NO3)2 6H2O, Zn(NO3)2 6H2O, and Fe(NO3)3 9H2O were dissolved in a minimal quantity of deionized water while the mixture was continuously stirred. After adding the predetermined quantity of hydrazinium acetate ligand solution slowly while swirling it constantly, the solution was fully combined after being properly mixed. After that, the mixture was placed on a hot plate to finish drying. The combination dried out to become a solid mass, which then auto-catalytically got degraded into the powder form. These powders were then employed for characterisation and investigation of the structural, electrical, and magnetic characteristics of the material. The Rigaku, X-ray advance Power diffractometer with Cu K radiation (= 1•54183) was used to carry out the structural evaluation of the generated Mg-Zn ferrite nanoparticles. This was done so in order to determine the nanoparticles' unique structural characteristics. The step size that was used was 0•02°, and the range that it covered was from 200 to 800. Infrared spectroscopy, sometimes known as IR, is one of the instruments that may be used for qualitative as well as quantitative investigation of different molecular species. It is used in conjunction with the intensity measurements for the purpose of identifying chemical and structural components, as well as for quantitative purposes. In the infrared spectrum, a chemical compound exhibits very pronounced selectivity in its absorption. After being exposed to infrared light, the molecules that make up chemical compounds begin to vibrate at various speeds, which results in the formation of a spectrum of closely packed absorption bands known as the IR absorption spectrum. The sample of solid ferrite was finely pulverised together with the pure and dry KBr in the usual experiment, with the ratio being 1:10. In order to ensure that the sample is thoroughly combined with the KBr, fine grinding is essential. After that, the mixture was transferred to a sample holder, and the sample holder was positioned within the sample chamber of the IR spectrophotometer. The spectra of the sample's absorption was recorded across the wavelength range of 1000 cm-1 to 400 cm-1. The experiment was performed many times with each of the samples. The Scherer formula was used to get the average particle size T based on the most intense peak (311), which was used in the calculation. The JEOL 5800LV Scanning Electron Microscope was used to conduct the experiments on the particle size and shape. All of the samples' saturation magnetization was measured using a Pulse Field Magnetic Hysteresis Loop Tracer, Model PFMHT-1, which was supplied by Magneta India. All of the measurements were carried out at room temperature. The hysteresis loops allowed for the derivation of the values for magnetization, coercivity, and remanence magnetization.

RESULTS AND DISCUSSION

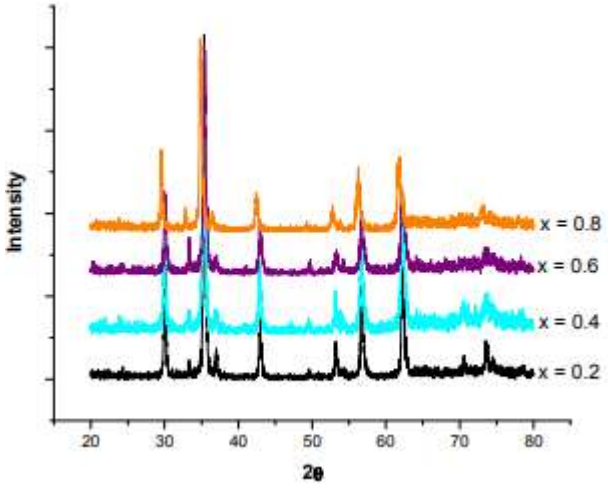

Figure 1: X-ray diffraction patterns of samples MgxZn1-x Fe2O4

The X-ray diffraction patterns of samples made up of MgxZn1-x Fe2O4, with x equal to 0.2, 0.4, 0.6, and 0.8 nanoparticles, are displayed in Figure 1. The creation of a single phase ferrite is demonstrated by the fact that each of the peaks corresponds to a cubic spinel ferrite structure for each of the samples.

Table 1: Variation of lattice constant for various Mg-Zn ferrite samples synthesised

samples	**a in cm**
$Mg_{0.2}Zn_{0.8}Fe_2O_4$	8.445×10^{-8}
$Mg_{0.4}Zn_{0.6}Fe_2O_4$	8.437×10^{-8}
$Mg_{0.6}Zn_{0.4}Fe_2O_4$	8.411×10^{-8}
$Mg_{0.8}Zn_{0.2}Fe_2O_4$	8.396×10^{-8}

Using the characteristic (311), the values for the lattice constants were obtained for all Mgx Zn(1-x)Fe2o4 nanoparticles. These calculations were performed using XRD patterns. Table 1 contains the values of the lattice constants, and Figure 2 illustrates how those values should be displayed. It has been discovered that the lattice constant, denoted by the letter a, decreases as the magnesium concentration rises. This drop in lattice constant may be related to the ionic size discrepancies, where Mg2+ ions, which have a smaller ionic size of 0.66, are substituted by Zn2+, ions with a higher ionic size of 0.82. As the concentration of Mg increases, the lattice constant decreases. Using the method presented in equation 1, we were able to determine the value of the lattice parameter known as "a" by utilising the values for the lattice spacing, or "d," and the respective miller indices, or "hkl." The values of the lattice parameters fall somewhere in the range of -8.445 to -8.396 angstroms.

$$a = d/ (h^2+k^2+l^2)^{1/2} \quad (1)$$

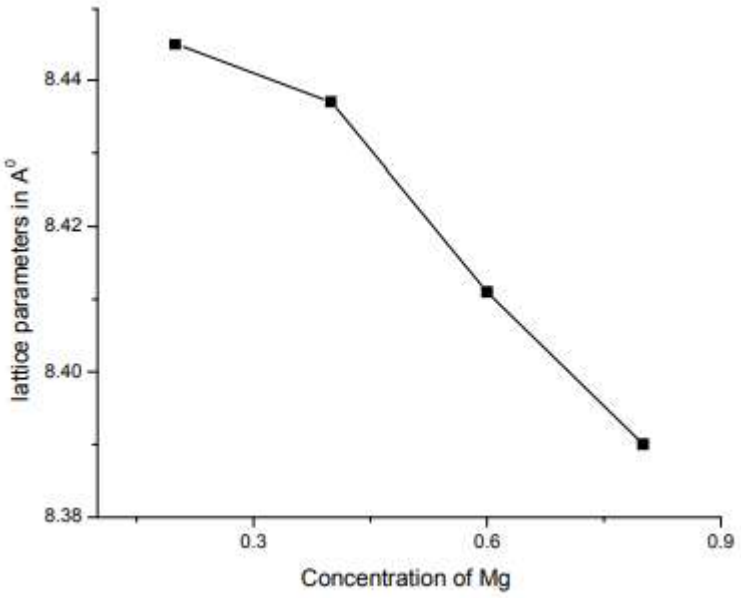

Figure 2 : variation of Lattice Constant with Conc. of Mg

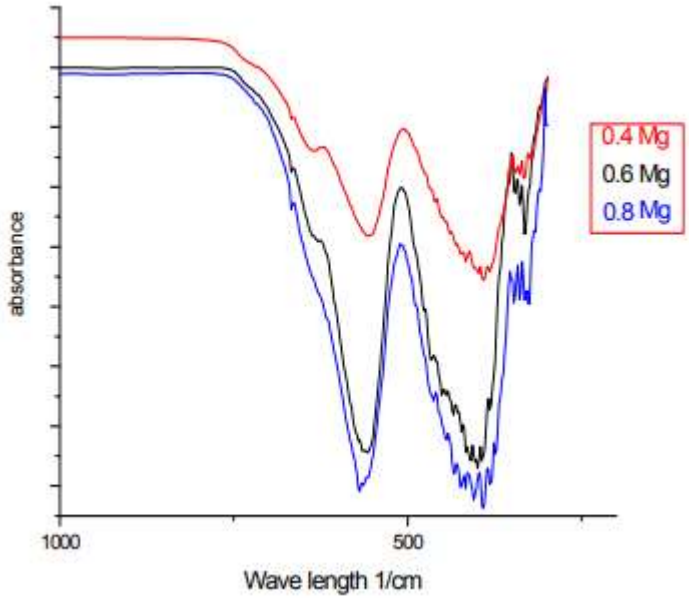

Figure 3: IR spectra of MgxZn1-x Fe2O4samples

The spinel structure may be determined with the use of infrared (IR) absorption spectroscopy. The first, second, and third characteristic vibrational bands related with the structure of spinel are located at (1) 600-550 cm-1; (2) 450-385 cm-1; and (3) 350-330 cm-1 for the metal-oxygen band. Studies of the nano particle ferrite samples using Fourier transformed infrared (FTIR) spectroscopy were carried out between 1000 and 400 cm-1, as shown in figure 3. The bands in the ranges of 600–550 cm-1 and 450–385 cm-1 in spinel ferrites are ascribed to tetrahedral and octahedral metal ions vibrations with oxygen ions, respectively. These bands, which are also distinctive bands of spinel ferrite, are seen in spinel ferrites. The presence of two strong absorption bands can be seen in figure 3, specifically v1 in the range of 566–555 cm-1 and 2 = 405–396 cm-1 for the samples that have been prepared in their original state. As a function of the amount of magnesium present, the band locations 1 and 2 are indicated in Table 2. The band 1 corresponds to the stretching vibration mode caused by the vibration of the chemical bond O–Mtet.–O in

the location of tetrahedral position, and the band 2 corresponds to the vibration of the chemical bond O–Moct.–O in the metal–oxygen vibration in octahedral sites. Both of these modes are caused by the vibration of the metal–oxygen bond. In ferrite samples, the creation of spinel structure may be deduced from the observation of these absorption bands when they are present. With an increase in magnesium content comes a shift toward higher wave numbers for the O–Mtet.–O band, as found by the researchers. There is a shift in a tetrahedral band of MgZn ferrite towards higher wave number as compared to the Zn ferrite, due to increasing Mg concentration, which gives an indication that preference of Mg ions in occupying tetrahedral lattice sites in addition to octahedral sites. This information was reported by some researchers. According to the research that has been done so far it is pretty clear that the Mg2+ ions in Mg ferrite nanoparticles have a strong preference for tetrahedral as well as octahedral positions.

Table 2: Variation of Wavelength.

Composition of Mg	Wavelength cm^{-1}	
	ν1	ν2
0.4	555	388
0.6	560	391
0.8	566	396

With the help of XRD data and the Scherer formula, average crystallite sizes were determined to be in the range of 20-44 nm for various Mg concentrations. This was accomplished by measuring the full-width at half maximum (FWHM) for each sample's most intense characteristic (311) peak, which was then used to calculate the average crystallite size.

$$T=0.9\ \lambda/D_p\cos\theta \qquad (2)$$

Where T represents the average size of a crystallite, represents the wavelength of X-rays, Dp represents the angular line width at which half of the maximum intensity is reached, and represents the Bragg angle in degrees. Table 3 provides information on the particle size of MgxZn1-x Fe2O4 nanoparticles with varying concentrations of Mg. The values for x range from 0.2 to 0.8. The diameters of the crystallites are all over the place and range from 20 to 44 nanometers for the various compositions. It has been discovered that the ferrite sample with a Mg content of x=0.8 has a minimum crystallite size of 20 nm. This may be because Mg2+ ions have a lower ionic radius than other ions.

Table 3: Variation of particle size

Samples	**Particle size in nm**
Mg0.2Zn0.8Fe2O4	44.1
Mg0.4Zn0.6 Fe2O4	41.9
Mg0.6Zn0.4 Fe2O4	32.8
Mg0.8Zn0.2 Fe2O4	20.5

As can be seen in Figure 4(a), (b) and (c), the microstructure of Mg- Zn ferrites reveal that the nanoparticles are agglomerated due to the presence of magnetic interactions and are of uniform grain size.

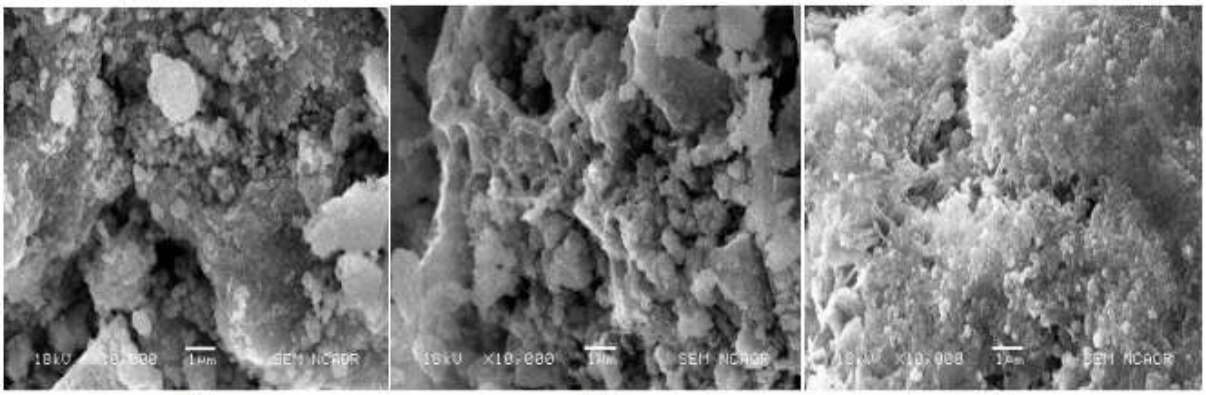

Figure 4: shows SEM images of MgxZn(1-x)Fe2o4 (x = 0.2,0.6 and 0.8) nanoparticles

The measurements of magnetization were performed using an applied magnetic field that reached a maximum strength of 5 kOe at room temperature. It was discovered that saturation magnetization went up as Mg concentration went up until x=0.6, but after that it went down for the sample with x=0.8, as shown in Figure 5. This was proven to be the case. Neel's two sub-lattice models, one of which posits a rise in resultant sublattice magnetic moment, can be used to provide an explanation for the first increase in saturation magnetization that occurs in response to an increase in the Mg content of the material. There were three different sorts of exchange interactions that were studied between the unpaired electrons of two ions that were occupying the A and B sites. The interaction between A and B is far more prevalent than the interactions between A and A and B and B. All of the magnetic spins at A sites are aligned in one way as a result of the interaction between A and B sites, while those at B sites are aligned in the other direction.

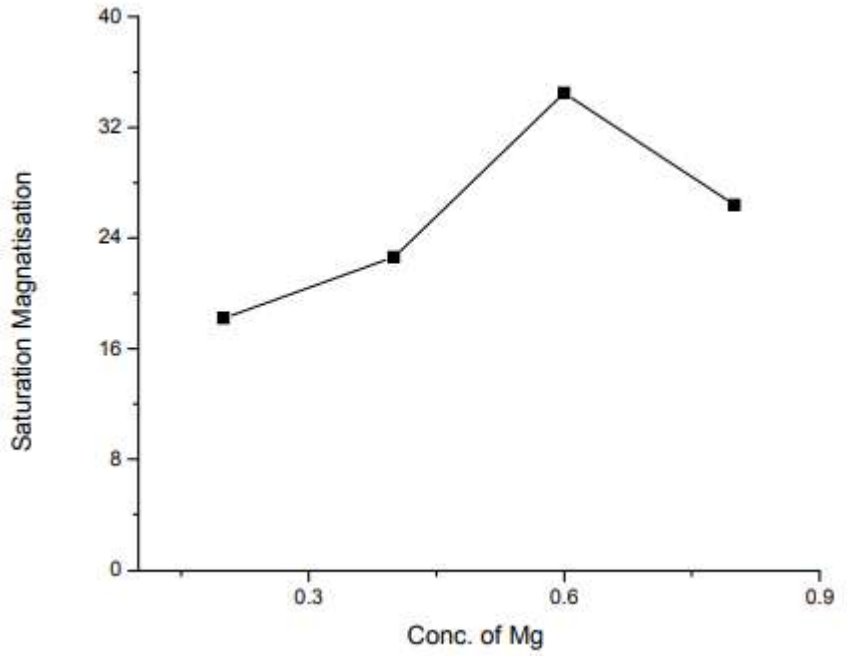

Fig 5: variation of saturation magnetization values of Mg-Zn ferrite

Therefore, the magnetic moments of the B and A sub-lattices are subtracted to determine the net magnetic moment of the lattice, denoted by the equation M = MB-MA. The magnetic moment of each composition is determined by the distribution of Fe3+ ions inside the A and B sub lattices. It is well known that the Mg-ferrite in nanoparticles form is a spinel with a certain degree of inversion and demonstrates magnetic behaviour due to its incomplete inverse spinel structure at nano-scale. The pure bulk Mg ferrite displays an inverse spinel structure, in which Mg2+ ions prefer octahedral sites. The distribution of Fe3+ ions on octahedral and tetrahedral lattice sites is the reason why there is a correlation between increased Mg concentration and an increase in the net magnetism. Because these Fe3+ ions are distributed in such a way, the A–B super exchange contacts are strengthened, which ultimately leads to an increase in the net magnetization. Since Mg2+ and Zn2+ ions are not magnetic by nature, the magnetization of Mg-Zn ferrite nanoparticles is dependent on the distribution of Fe3+ ions among tetrahedral and octahedral lattices sites. This is due to the fact that Mg-Zn ferrite nanoparticles are composed of tetrahedral and octahedral lattices.

Table 4: Saturation Magnetization values of Mg-Zn ferrite

Samples	Saturation Magnetization (emu/g)	Coercivity Hc	Retentivity Mr
$Mg_{0.2}Zn_{0.8}Fe_2O_4$	18.2	112.7	1.65
$Mg_{0.4}Zn_{0.6}Fe_2O_4$	22.6	104.9	2.42
$Mg_{0.6}Zn_{0.4}Fe_2O_4$	34.5	119.1	3.64
$Mg_{0.8}Zn_{0.2}Fe_2O_4$	26.4	111.5	2.96

The breakdown of the collinear ferromagnetic phase occurs at x = 0.6 when the amount of nonmagnetic Mg2+ ions continues to rise. This is caused by a rising dilution in A sites as a result of this phenomenon. Additionally, for Mg-Zn ferrite with x equal to 0.8, the triangular spin arrangement on B-sites is appropriate, and this results in a decrease in the amount of interaction between A and B and an increase in the amount of interaction between B and B. As a result, the drop in saturation magnetization may be described using the Yafet-Kittle model with three sub-lattice structures. As the magnesium content is raised from 0.2 to 0.8, there is a corresponding fluctuation in the coercivity, denoted by Hc, within the range of 100–120 Oe. The soft magnetic nature of these ferrite nanoparticles is shown by lower coercivity values, which also suggest the presence of ferromagnetic behaviour at room temperature for all of the samples that were synthesised in their natural state.

CONCLUSION

The purpose of the current research was to synthesise tiny particles of a Mg-Zn mixed metal ferrite material using the formula $Mg_xZn_{1-x}Fe_2O_4$ with x equal to 0.2, 0.4, 0.6, and 0.8. The samples were synthesised using a wet chemical approach. The samples were collected at a low temperature, and their characteristics were validated using a variety of techniques, including IR spectral analysis, XRD analysis, and scanning electron microscopy analysis. The samples have a lattice constant that falls anywhere in the

range of 8.445A0 to 8.396A0. The figures are almost exactly the same as the ones that were reported. Using the Scherer formula, we determined that the average particle size fell somewhere in the range of 20 nm to 44 nm. Saturation magnetization (Ms) values of samples are found to increase as magnesium content increases, up to Mg content x = 0.6, and decreased for x -0.8. This is attributed to the change in the cationic distribution at tetrahedral and octahedral sites. Saturation magnetization (Ms) values of samples are found to increase as magnesium content increases, up to Mg content x = 0.6. This Mg-Zn mixed metal ferrite exhibited weak magnetic properties, as demonstrated by low values of the coercivity parameter. It is therefore possible to draw the conclusion that the diverse changes that take place in the characteristics of Mg–Zn ferrite nanoparticles are attributable to the rearrangements of Mg and Zn divalent metal cations at various lattice locations.

REFERENCES

1. I Sharifi; H Shokrollahi; S Amiri. J. Magn. Magn.Mater., 2012, 324, 903–915.
2. N Gupta; A Verma; SC Kashyap; DC Dube. J. Magn. Magn. Mater., 2007, 308,137–142.
3. M Srivastava; A K Ojha; S Chaubey; A Materny. J. Alloys and Compounds, 2009, 481, 515. [4] N Gupta; A Verma; SC Kashyap; DC Dube. J. Magn. Magn. Mater., 2007, 308, 137–142.
4. T FBarth; E Posnjak. Z Krist., 1952, 82,325.
5. E Rezlescu; E L Sachelarie; N Rezlescu. J. Optoelectronics and Advanced Materials, 2006, 8, 1019–1022. [7] M A El Hiti; A I El Shora; SM Hammad. Mater. Sci. Technol., 1997, 13.
6. T Nakamura; Y. Okano. J. Phys. IV Fr., 1997, 7 (C1), 101.
7. K P Thummer; MC Chhantbar; KB Modi; GJ Baldha; H H Joshi. J. Magn. Magn. Mater., 2004, 280, 23–30.
8. J Smit; HPJ Wijn. Ferrites, Wiley, New York, 1959, p. 143.
9. Y Ichiyanagi; M Kubota; S Moritake; Y Kanazawa; T Yamada; T Uehashi. J. Magn. Magn. Mater., 2007, 310, 2378.
10. H Spiers; I P Parkin; Q A Pankhurst; L Affleck; M Green; D J Caruana; M V Kuznetsov; J Yao; G Vaughan; A Terry; A Kvick. J Mater. Chem., 2004, 14, 1104–1111.
11. R D Waldron. Phys. Rev., 1955, 99, 1727.
12. S J Keny; J Manjanna; G Venkateswaran; R Kameswaran. Corrosion Science 2006, 48, 2780–2798.
13. A Pradeep; P Priyadharsini; G Chandrasekaran. J. Magn. Magn. Mater., 2008, 320, 2774. I Neel. Ann. Phys., 1948, 3, 137.
14. A Goldman. Modern Ferrite Technology, second ed., Springer, New York, 2006.
15. M Ajmal; A Maqsood. J. Alloy. Comp., 2008, 460,54-59.